National Renewable Energy Laboratory

Innovation for Our Energy Future

Battery Thermal Management System Design Modeling

G.H. Kim and A. Pesaran

Presented at the 22nd International Battery, Hybrid and Fuel Cell Electric Vehicle Conference and Exhibition (EVS-22) Yokohama, Japan October 23–28, 2006

NOTICE

The submitted manuscript has been offered by an employee of the Midwest Research Institute (MRI), a contractor of the US Government under Contract No. DE-AC36-99GO10337. Accordingly, the US Government and MRI retain a nonexclusive royalty-free license to publish or reproduce the published form of this contribution, or allow others to do so, for US Government purposes.

This report was prepared as an account of work sponsored by an agency of the United States government. Neither the United States government nor any agency thereof, nor any of their employees, makes any warranty, express or implied, or assumes any legal liability or responsibility for the accuracy, completeness, or usefulness of any information, apparatus, product, or process disclosed, or represents that its use would not infringe privately owned rights. Reference herein to any specific commercial product, process, or service by trade name, trademark, manufacturer, or otherwise does not necessarily constitute or imply its endorsement, recommendation, or favoring by the United States government or any agency thereof. The views and opinions of authors expressed herein do not necessarily state or reflect those of the United States government or any agency thereof.

Available electronically at http://www.osti.gov/bridge

Available for a processing fee to U.S. Department of Energy
and its contractors, in paper, from:
      U.S. Department of Energy
      Office of Scientific and Technical Information
      P.O. Box 62
      Oak Ridge, TN 37831-0062
      phone: 865.576.8401
      fax: 865.576.5728
      email: mailto:reports@adonis.osti.gov

Available for sale to the public, in paper, from:
      U.S. Department of Commerce
      National Technical Information Service
      5285 Port Royal Road
      Springfield, VA 22161
      phone: 800.553.6847
      fax: 703.605.6900
      email: orders@ntis.fedworld.gov
      online ordering: http://www.ntis.gov/ordering.htm

Printed on paper containing at least 50% wastepaper, including 20% postconsumer waste

BATTERY THERMAL MANAGEMENT DESIGN MODELING

Gi-Heon Kim

Post Doctoral Researcher, National Renewable Energy Laboratory, 1617 Cole Blvd, Golden, Colorado 80401 USA, +1 303 275-4437, Fax: +1 303 275-4415, gi_heon_kim@nrel.gov

AHMAD A. PESARAN

Principal Engineer, National Renewable Energy Laboratory, 1617 Cole Blvd, Golden, Colorado 80401 USA, +1 303 275-4441, Fax: +1 303 275-4415, ahmad_pesaran@nrel.gov

Abstract

Battery thermal management is critical in achieving performance and extended life of batteries in electric and hybrid vehicles under real driving conditions. Appropriate modeling for predicting thermal behavior of battery systems in vehicles helps to make decisions for improved design and shortens the development process. For this paper, we looked at the impact of cooling strategies with air and both direct and indirect liquid cooling. The simplicity of an air battery cooling system is an advantage over a liquid coolant system. In addition to lower heat transfer coefficient, the disadvantage of air cooling is that the small heat capacity of air makes it difficult to accomplish temperature uniformity inside a cell or between cells in a module. Liquid cooling systems are more effective in heat transfer and take up less volume, but the added complexity and cost may outweigh the merits. Surface heat transfer coefficient, h, and the blower power for air cooling are sensitive to the hydraulic diameter of the channel (D_h). However, because of the added thermal resistances, h evaluated at cell surface is not as sensitive to the variation of D_h in a water/glycol jacket cooling system. Due to the high heat transfer coefficient at small D_h and large coolant flow rate, direct liquid cooling using dielectric mineral oil may be preferred in spite of high pressure loss in certain circumstances such as in highly transient large heat generating battery systems. Results of computational fluid dynamics (CFD) model simulation imply that capturing the internal heat flow paths and thermal resistances inside a cell using a sophisticated three-dimensional cell model are important for the improved prediction of cell/battery thermal behaviors. This paper identified analyses and approaches that engineers should consider when they design a battery thermal management system for vehicles.

Introduction

Temperature greatly affects the performance and life of batteries, so battery thermal control must be used in electric and plug-in hybrid electric vehicle under real driving conditions. In recent years, automakers and their battery suppliers have paid increased attention to battery thermal

management, especially with regard to life cycle and related warranty costs. A thermal management system could be designed with a range of methods, from "simple energy balance equations" to more "sophisticated thermal and computational fluid dynamics models." Regardless of the method, the basic performance of the management system is dictated by the thermal design of each cell or module.

Designing a battery thermal management system for given HEV/PHEV battery specifications starts with answering a sequence of questions: "How much heat must be removed from a pack or a cell?" "What are the allowable temperature maximum and difference?" "What kind of heat transfer fluid is needed?" "Is active cooling required?" "How much would the added cost be for the system?" etc. In order to find a high performance and cost effective cooling system, it is necessary to evaluate system thermal response and its sensitivity as a function of controllable system parameters.

The diagram below shows the working flow chart of our battery thermal management modeling process. Cell characteristics (dimensions, geometry, electrochemistry), operating conditions (power load from the vehicle, ambient conditions), module/pack cooling strategy (active or passive, air or liquid cooling, flow rates and temperature duty cycle) are all input to the battery thermal design management model. The model uses these inputs to do component and system analysis to predict the thermal response of the design. Modifications to the design can then be evaluated to determine the optimum solution considering factors such as cost, volume, mass, and maintenance issues.
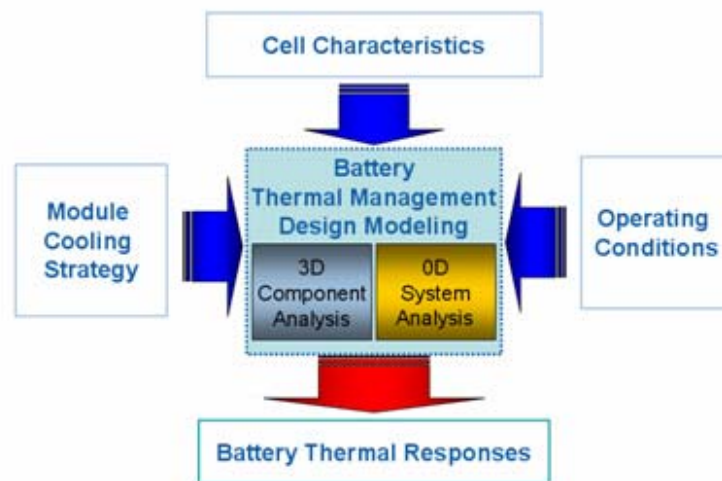
Analysis and Results

A typical parallel cell cooling system was investigated as an example study. Figure 1 presents the schematics of a system configuration and system thermal responses. Pressure loss in coolant channel (ΔP), coolant temperature change between channel inlet and outlet (ΔT_1), and temperature difference between cell surface and coolant mean temperature (ΔT_2) are chosen for

the system responses of interest. ΔP and coolant flow rate determine the required pump/blower power and size. ΔT_1 is a parameter indicating cell temperature uniformity possibly achieved. ΔT_2 is closely related to heat transfer coefficient, h, and shows how much the cell temperature would be higher than the coolant temperature. On the other hand, maximum cell surface temperature relative to coolant inlet temperature, $\Delta T_{max} = \Delta T_1 + \Delta T_2$, can be used as a parameter for controlling the upper limit of cell temperature tolerance.
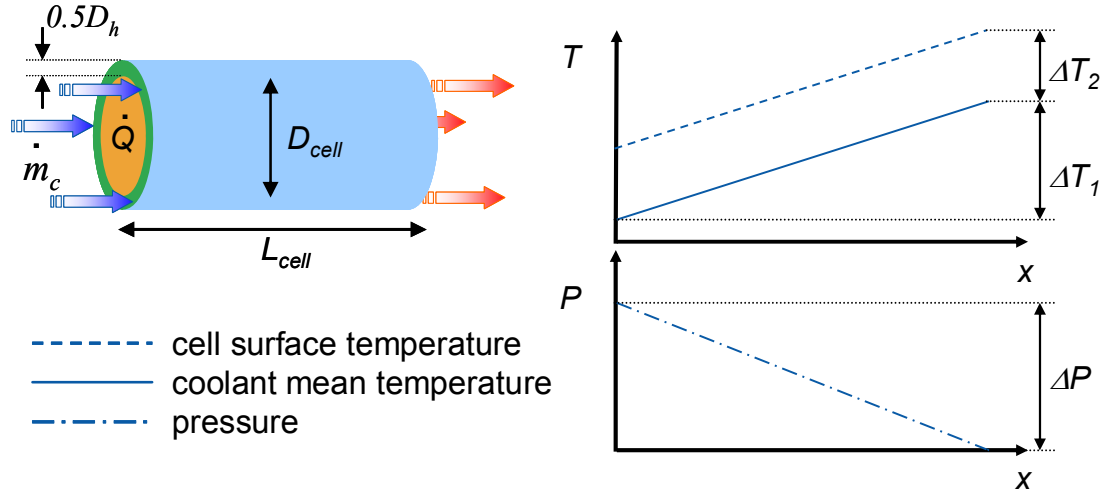

Figure 1: Schematics of a typical parallel cell cooling system and system responses

Note that the cell internal temperature distribution and its maximum depend on the thermal paths and resistances inside a cell. Therefore, the shapes, materials, thermal connectivity of cell components and location of heat transfer are important for predicting cell internal temperatures. Detailed investigations into this topic have been covered in separated studies. The effects of using different types of coolants were examined here. (See Table 1 for the properties of the heat transfer fluids examined here; air and dielectric mineral oil for direct cooling, and water/glycol for jacket cooling.) We selected coolant mass flow rate ($\dot{m}_c$) and the hydraulic diameter of coolant channels (D_h) as system control parameters. In this example case study, the cell was specified to have a 50 mm diameter, a 100 mm length, and to generate 2 *W* of heat.

Even though the heat transfer is enhanced in a turbulent flow regime, the required blower power greatly increases with laminar to turbulence flow-transition. Therefore, many heat exchanger applications are designed to be operated at laminar flow regimes. If the channel gap is much smaller than cell diameter, the following fully developed laminar flow relations can be applied to the presented system.

$$c_f \mathrm{Re} = 24 \qquad\qquad\qquad\qquad (\text{Eq. 1})$$
$$\mathrm{Nu} = 5.385$$

where $\mathrm{Re} = V D_h / \nu$, $\mathrm{Nu} = h D_h / k$ and c_f is friction coefficient. The Nuselt number is evaluated for constant heat flux wall boundary conditions.

Table 1: Properties of coolants typically used in battery cooling systems

Coolant / Property	Air	Mineral Oil	Water/Glycol
Density ρ (kg/m^3)	1.225	924.1	1069
Specific Heat c_p ($J/kg\ K$)	1006.43	1900	3323
Thermal Conductivity k ($W/m\ K$)	0.0242	0.13	0.3892
Kinematic Viscosity ν (m^2/s)	1.461e-5	5.6e-5	2.582e-6

Figure 2 (a) shows the channel pressure losses per unit mass flow rate ($\Delta P / \dot{m}_c$) as a function of the coolant channel hydraulic diameter of coolant channel for different coolants. Due to the large difference in kinematic viscosity, ΔP varies in very different ranges for each coolant fluid. ΔP is directly proportional to fluid kinematic viscosity (ν) and coolant mass flow rate ($\dot{m}_c$). If the cell diameter is much larger than D_h, ΔP becomes inversely proportional to D_h^3. Therefore the channel pressure loss changes are very sensitive to D_h when it is small, especially for the high kinematic viscosity fluids.

$$\Delta P \sim \frac{\dot{m}_c \nu}{D_h^{\ 3}} \qquad\qquad\qquad\qquad \text{(Eq. 2)}$$

$$\frac{\partial \Delta P}{\partial D_h} \sim -\frac{\dot{m}_c \nu}{D_h^{\ 4}}$$

Flow power requirements to overcome the channel friction loss were normalized by the square of coolant mass flow rate and compared for the different coolant systems in Figure 2(b). Due to the much smaller fluid density and consequently larger volumetric flow rate at given mass flow rate, the air cooling system requires much higher flow power for compensating channel friction loss than the other systems at the given coolant mass flow rate and channel height. Note that not only the coolant channel friction loss but also the system manifold friction head and the static pressure head make a significant contribution to the required pumping power in liquid cooling systems.
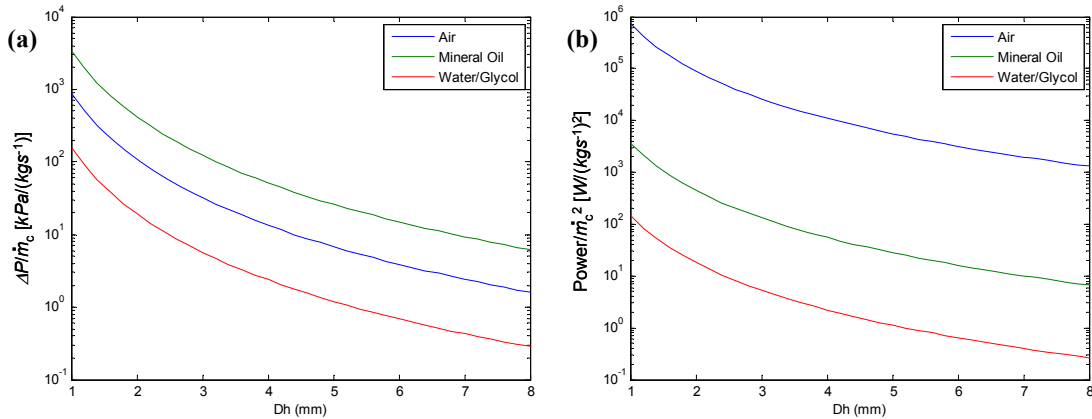

Figure 2: (a) Channel pressure loss per unit mass flow rate as a function of the coolant channel hydraulic diameter. (b) Flow power requirement for pressure loss normalized by square of mass flow rate as a function of the coolant channel hydraulic diameter.

Variations of ΔT_1 and ΔT_2 are shown for $\dot{m}_c$ and D_h respectively in Figure 3. To achieve the temperature uniformity over a cell, it is preferred to keep coolant temperature change in the channel as small as possible. ΔT_1 is inversely proportional to coolant heat capacity flow rate. Therefore, increasing mass flow rate is not as effective in reducing coolant temperature change in large flow rate cooling as it is in a small flow rate region. In other words, in small flow rate cooling, a little change in flow rate can greatly affect the coolant temperature change, and consequently cell temperatures (especially when air is used for the heat transfer medium that has small c_p as compared in Figure 3). Water/glycol is the most preferred among the tested coolant materials for achieving temperature uniformity of cell/pack due to its large heat capacity.

$$\Delta T_1 \sim \frac{1}{\dot{m}_c c_p} \qquad\qquad\qquad \text{(Eq. 3)}$$

$$\frac{\partial \Delta T_1}{\partial \dot{m}} \sim -\frac{1}{c_p}\frac{1}{\dot{m}_c^{\,2}}$$

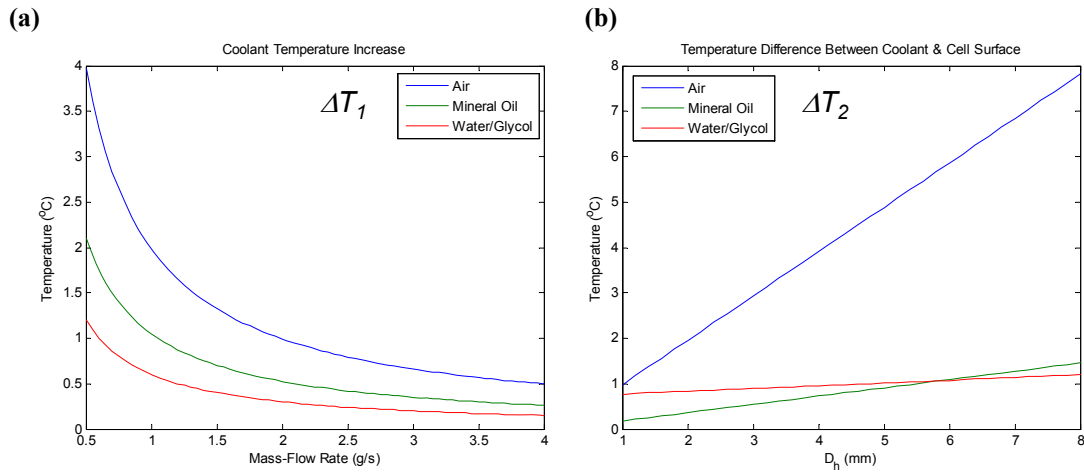**(a)**   **(b)**

Figure 3: (a) Variation of coolant temperature change inside a system as a function of coolant mass flow rate. (b)Variation of temperature difference between coolant and cell surface as a function of hydraulic diameter of coolant channel.

Temperature difference between coolant flow and cell surface, ΔT_2, is linear to D_h with slope being proportional to $1/k$ as shown in Figure 3. Note that 0.7 mm jacket wall thickness and 0.05 mm air layer were considered between cell surface and water/glycol coolant channel. Due to small thermal conductivity of air, ΔT_2 rapidly increases with D_h in air cooling. Therefore, if a small ΔT_2 (or large heat transfer coefficient) is required, it is recommended to use the smallest hydraulic diameter channel possible for air cooling. On the other hand, ΔT_2 is not so sensitive to variations of D_h in water/glycol cooling system due to relatively large thermal conductivity.

$$\Delta T_2 \sim \frac{1}{k}D_h + const \qquad\qquad\qquad \text{(Eq. 4)}$$

Note that *const* is 0 for direct contact cooling in the relation shown above.

The ΔT_2 curve shown in Figure 3 also implies heat transfer coefficient, h, which is inversely proportional to ΔT_2. h is plotted as a function of D_h in Figure 4. In steady state, high h lowers ΔT_2 to reduce cell temperature. In unsteady heat transfer viewpoint, high h means fast heat removal from small temperature displacement, reducing the peak temperature of the cell. Therefore, high h

smoothes out the cell temperature oscillations under transient heat generating conditions. The heat transfer coefficient evaluated at cell surface for water/glycol jacket cooling greatly decreases compared with the value it would be if direct contact cooling due to added thermal resistances between coolant and cell. The reduction is greater at small D_h. So, direct liquid cooling using mineral oil shows much higher h values than the other coolants at D_h <2~3 mm in the presented case. In spite of large pressure losses due to large v and small D_h in this operating region, mineral oil cooling may be preferred for its high heat transfer coefficient in certain conditions.
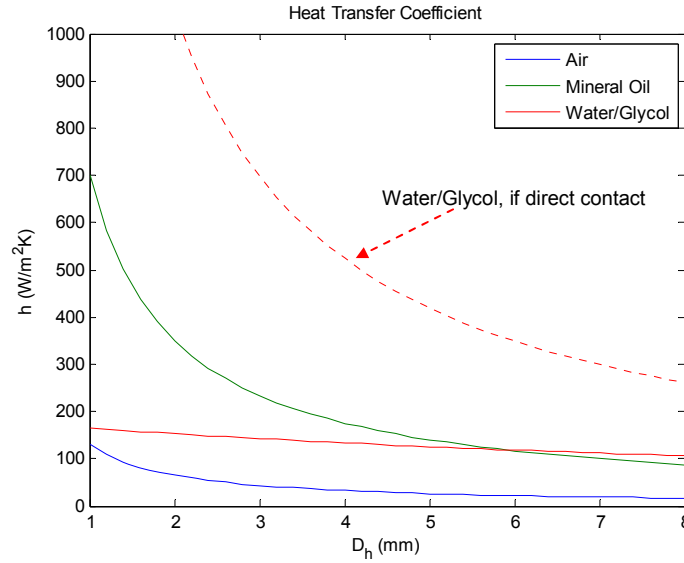
Figure 4: Variation of heat transfer coefficient as a function of coolant channel hydraulic diameter.

Contours of maximum cell surface temperature relative to coolant inlet temperature, ΔT_{max} ($=\Delta T_1+\Delta T_2$) are plotted as a function of coolant mass flow rate ($\dot{m}_c$) and hydraulic diameter of coolant channels (D_h) for different coolant systems. The values of ΔT_{max} in the air system are much higher compared with other fluid systems due to its small heat capacity and thermal conductivity. Contour lines for the air system, Figure 5(a), are dense and mostly aligned vertically at $\dot{m}_c$ > ~ 1 g/s. This means that ΔT_{max} is dominated by and sensitive to D_h in this operating region. On the other hand, the water/glycol jacket cooling system (Figure 5(c)) contour lines are almost horizontal at $\dot{m}_c$ < ~ 2 g/s, and the line density is relatively sparse at $\dot{m}_c$ > ~ 2 g/s. This means that ΔT_{max} is not very sensitive to D_h, and that ΔT_{max} would not be a strict limiting design factor of the water/glycol system. The lowest value of ΔT_{max} appears in the mineral oil direct contact cooling system (Figure 5(b)) with a small D_h and large $\dot{m}_c$ operating region. Note that great pressure loss occurs in that operation region.
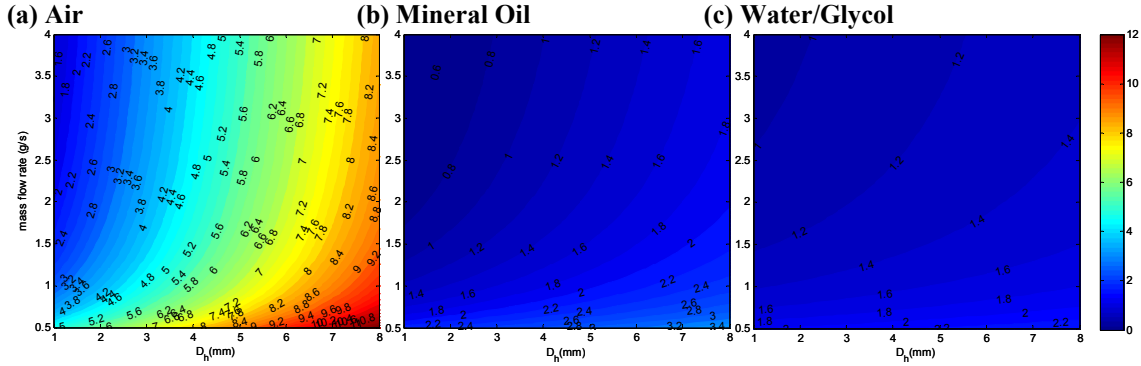
Figure 5: Contours of maximum cell surface temperature relative to coolant inlet temperature

An example of confining the operation zone to given conditions is shown in Figure 6. By drawing contour lines of required conditions, possible operating zones can be found. The colored area shown in Figure 6 represents the operating zone satisfying Re<2300, ΔP<110 *Pa*, ΔT_{max}<4.5 ^{o}C and ΔT_{l}<1.5 ^{o}C in an air cooling system. Laminar restriction of Reynolds number is to avoid excessive friction loss due to turbulence flow transition. Point **A** is the operating point for getting maximum *h* for given conditions. **B** is the lowest ΔT_{max} operating point, and **C** is the minimum pressure loss (ΔP) operating point.
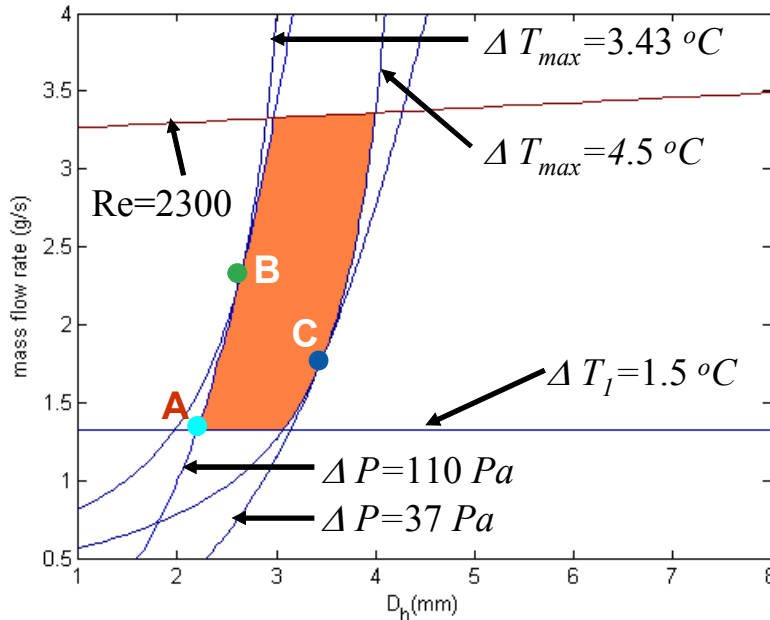
Figure 6: Confining the operation zone and parameter optimization to given conditions

An operating point (D_h , $\dot{m}_c$) = (2.2 mm, 1.33 *g/s*) which is close to point **A** in Figure 6, the maximum *h* operating point satisfying given limiting conditions, was selected and simulated for the air cooling system using an axi-symmetric computational fluid dynamics (CFD) model. The model geometry and mesh are presented in Figure 7. The model includes internal cell component materials and geometries. The cell core winding was treated as a continuous material having orthotropic properties according to layer directions. As specified previously, the cell is 50 mm in diameter, 100 mm in length and generates heat with a rate of 2 *W* at its core. Inlet air temperature

7

was set to 35 ^{o}C. The other surfaces, except the channel/cell interface were set as thermally adiabatic boundaries.

Figure 8 shows temperature distribution contours of the cell and cooling air. In the upper frame of the figure, radial-direction length scale is exaggerated to see the thermal development in the air channel. Cell surface temperature constantly increases in the axial direction as coolant air temperature increases. However, cell internal temperature distribution is determined by the thermal paths and thermal resistances inside a cell. The maximum temperature of 38.41 ^{o}C appears on the cell axis a little bit downstream from the cell center in the presented cell specification.
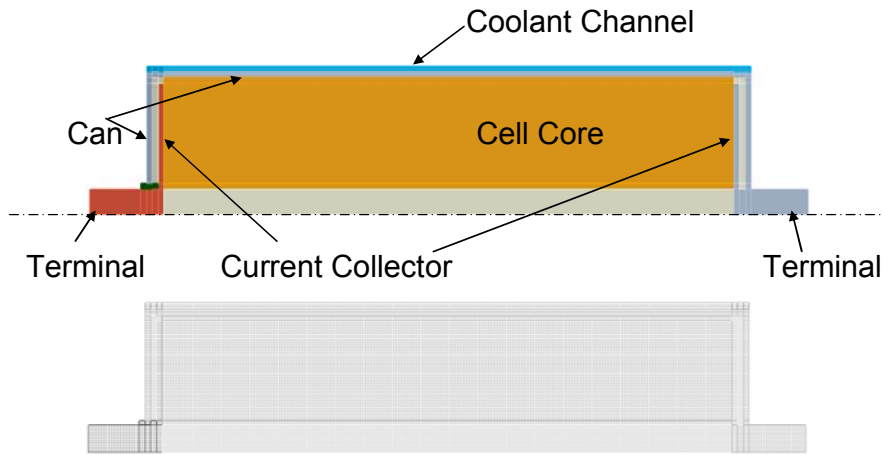
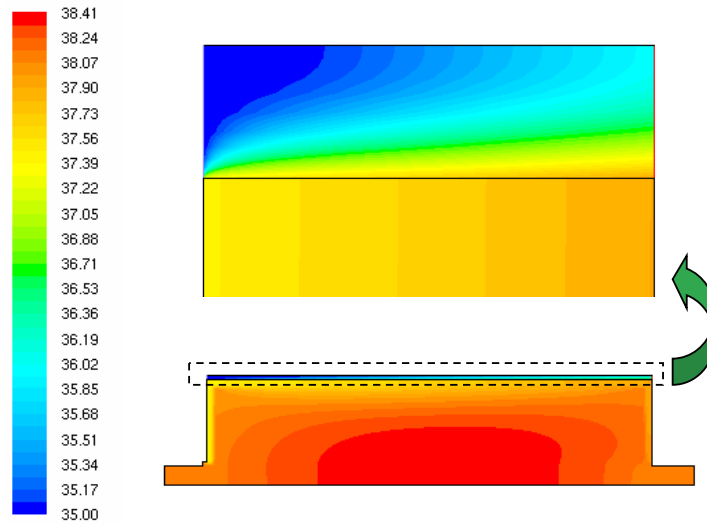**Figure 7: Model geometry and mesh representing an axisymmetric cylindrical cell**

**Figure 8: Temperature distribution contours of the cell and the air coolant channel
(top: expanded view near can surface and coolant channel)**

Axial distribution of air flow mean temperature, cell surface temperature and cell center-line temperature are presented in Figure 9. Coolant air temperature change, ΔT_l, is computed as 1.50 ^oC. The maximum cell surface temperature relative to inlet air temperature, ΔT_{max}, is 2.89 ^oC at the channel outlet. The highest battery temperature appears in the middle of the centerline of the cell and displaced from coolant inlet temperature by 3.41 ^oC. Due to entrance effect, air temperature rapidly increases near the channel inlet. In the entrance region, the radial profiles of temperature and velocity at the cell/coolant interface have steep gradients representing higher heat flux and wall friction. Entrance effect is more clearly seen on the axial distribution of heat transfer coefficient (h) and heat flux shown in Figure 10.
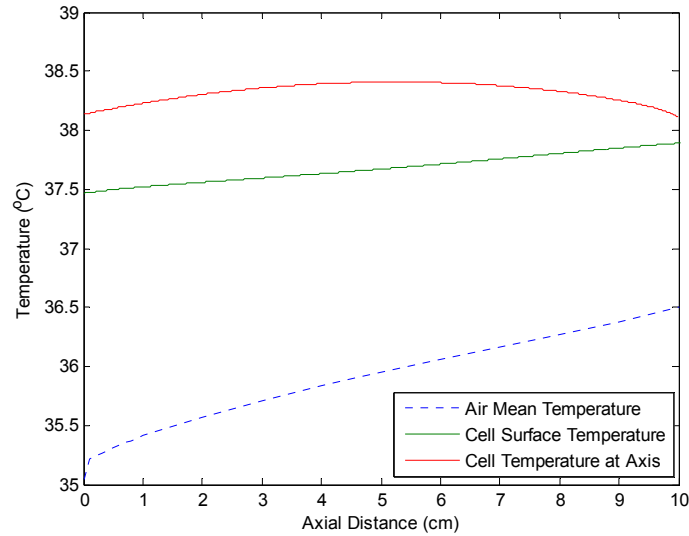
Figure 9: Axial distribution of air flow mean temperature, cell surface temperature and cell center-line temperature
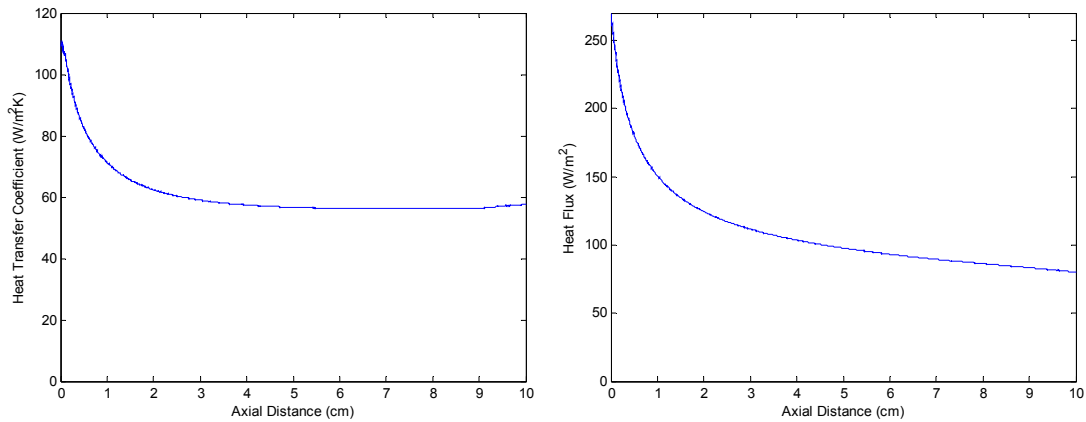
Figure 10: Axial distribution of heat transfer coefficient and heat flux

Heat transfer coefficient, h, at the cell surface has a larger value near the channel inlet, and consequently so does the heat flux. As the flow approaches fully developed, the value of h converges to the constant value, 56.23 W/m^2K, which is slightly lower that the predicted value, 59.24 W/m^2K, using the relations shown in Eq. 1. However, the mean value of h over the heat transfer surface has a little bit higher value, 60.96 W/m^2K, due to the entrance zone effect. One of

9

the reasons for this discrepancy comes from the fact that heat flux distribution is not quite constant along the axial distance. Heat flux decreases continuously with axial distance so that the cell surface temperature increases slowly compared to coolant air mean temperature as shown in Figure 9 (see the difference of slopes of two curves).

System response parameters from different prediction methods are presented in Table 2. Even though ΔP is predicted to be a little bit higher in CFD analysis due to the entrance effect, the parameters are generally well matched between the prediction methods except for the maximum cell surface temperatures. The disagreement of ΔT_{max} mainly originates from the fact that CFD analysis can capture the axially decreasing heat flux from cell to air, which makes the axial gradient of cell surface temperature smaller than that of air temperature. This is because high conductivity materials inside a cell, such as the aluminum can, would transfer internal heat flow to make cell temperature more even. This result strongly implies that capturing the internal heat flow paths and thermal resistances inside a cell are important for the improved prediction of cell/battery thermal behaviors.

Table 2: System response parameters - Two different prediction methods

	ΔP [Pa] channel pressure loss	ΔT_1 [ºC] coolant temperature change	ΔT_{max} [ºC] maximum cell surface temperature to inlet air	ΔT_{cell} [ºC] maximum cell internal temperature to inlet air	$\bar{h}$ [W/m²K] mean heat transfer coefficient
Fully Developed Flow Relations with Constant Heat Flux	109.1	1.49	3.64	N/A	59.24
CFD	114.2	1.50	2.89	3.41	60.96

Cooling of a larger cell that has 50 mm diameter, 200 mm length and generates heat with a rate of 4 W at the cell core was simulated for a direct air cooling system and a water/glycol jacket cooling system. Reducing channel height greatly increases heat transfer coefficient at cell surface in a direct contact air cooling system. But reducing the channel height is limited by the channel friction loss, which increases sensitively with decreasing D_h for a given coolant flow rate. On the other hand, in an indirect water/glycol liquid cooling system, channel height is not a sensitive factor affecting heat transfer coefficient at cell surface as it is in air systems, even though water/glycol channel friction loss is not as significant in magnitude as in air for a given coolant mass flow rate. But it is still recommended in a liquid cooling system to use a small gap coolant channel to reduce system weight and volume by minimizing the amount of coolant in a system operated at a given coolant flow rate. CFD analyses were carried out for a direct air cooling system operated at (D_h, $\dot{m}_c$) = (2.2 mm, 1.33 g/s) and for a water/glycol jacket cooling system at (D_h, $\dot{m}_c$) = (4.0 mm, 1.70 g/s) as shown in Figure 11. Inlet coolant temperatures were set to 35 ºC. The results indicate that due to the large differences of coolant velocity and kinematic viscosity between the two systems, the air cooling system needs to compensate for a much larger pressure loss than the water/glycol liquid cooling system (221 Pa versus 7.68 Pa).
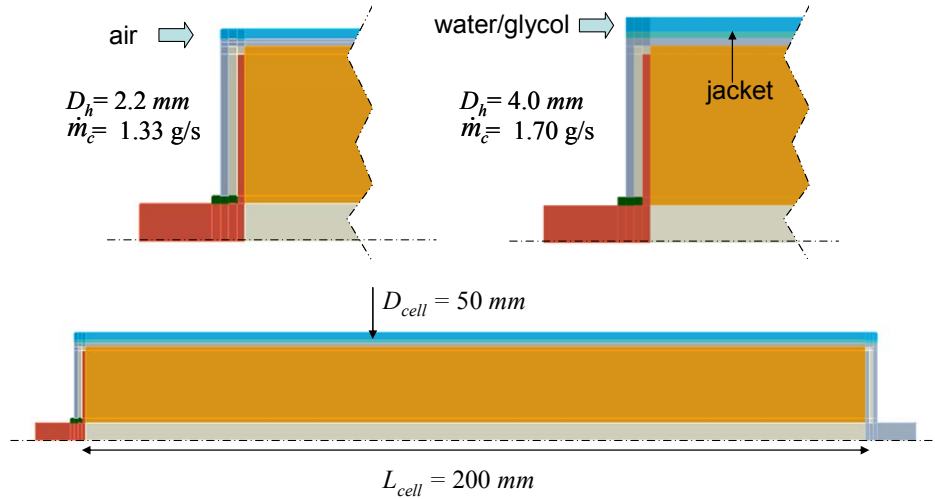
Figure 11: Schematics of larger cell geometries and coolant channels

Temperature distribution contours are shown for comparison in Figure 12. Even though the rate of heat removal from cell to coolant is the same for the two compared systems, air flow is rapidly heated compared with water/glycol due to the small heat capacity of air. In addition, the difference between coolant mean temperature and cell surface temperature is larger in the air cooling system because of the smaller heat transfer coefficient. Therefore, not only the maximum temperature but also the temperature non-uniformity inside a cell is larger in the air cooling system than in the water/glycol system. Temperature imbalance inside a cell is bigger in the air cooling system. Note that temperature contour-lines are distributed similarly inside a cell in both cases. This implies that internal heat flows are similar in both systems, and consequently that the internal heat paths and the thermal resistances are determining the relative temperature distribution inside a cell.
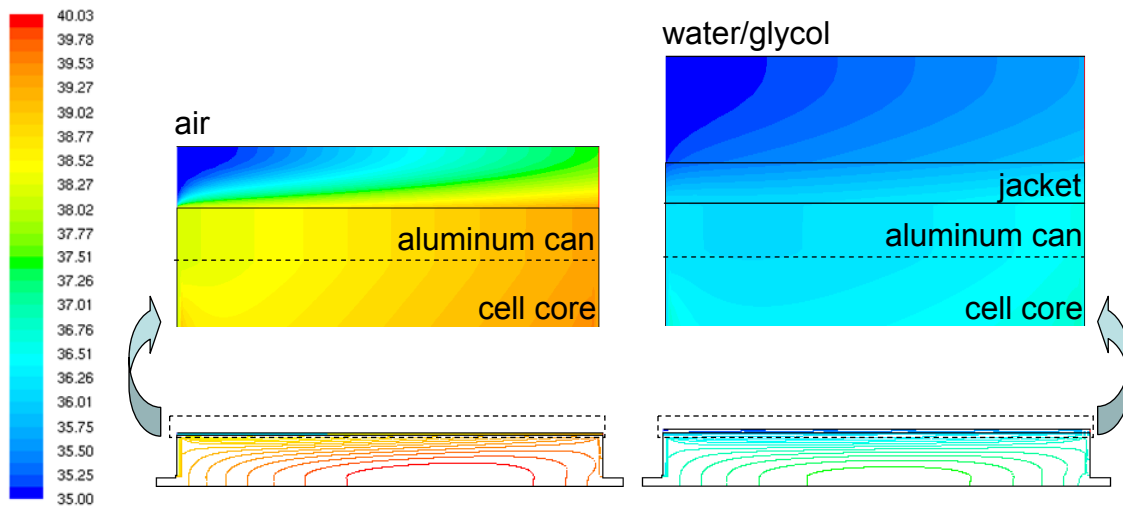

Figure 12: Comparison of temperature distribution contours between air cooled cell and water/glycol cooled cell

Axial temperature profiles of the air cooling system and the water/glycol system are compared in Figure 13 (a). Compared with the water/glycol liquid cooled cell, the maximum temperature on the cell axis in the air cooled cell appears near the channel exit. A larger temperature difference between each end of the cell shifts the maximum temperature location further downstream. Heat transfer coefficients at cell surfaces are plotted in Figure 13 (b) for both systems.

$$h = \frac{q''}{T_{cell\_surf} - \overline{T}_{coolant}} \tag{Eq 5}$$

Thermal resistances of the jacket wall and air gap layer between the channel coolant and the cell surface were used to evaluate the heat transfer coefficient of the water/glycol cooling system. Temperature displacement between the channel surface and the cell surface in the water/glycol cooled cell shown in Figure 13 (a) is due to these added thermal resistances. The higher heat transfer coefficient of the water/glycol system leads to a smaller temperature difference between the coolant and cell surface as shown in Figure 13 (a) and Eq. 5. Even though the cell temperatures are distributed in different ranges in each system, the magnitudes of temperature differences between the cell center axis and the cell surface of the air cooled cell and the water/glycol cooled cell are not very different because the same cell specifications are assumed for both cases.
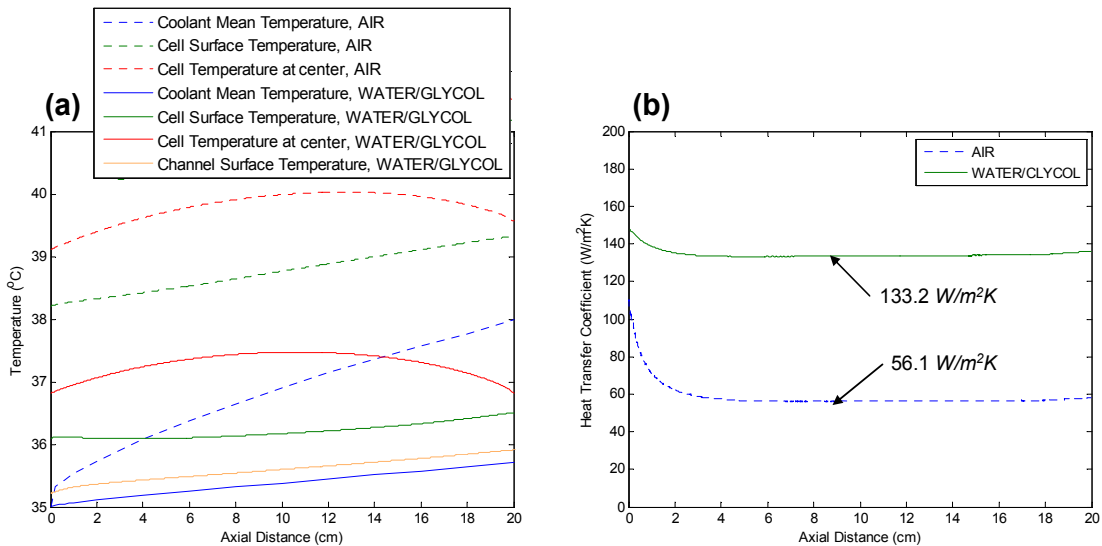

Figure 13: Axial profiles of temperatures (a) and heat transfer coefficients at cell surfaces (b)

A serial cooling system may be preferred over a parallel cooling system for its simplicity of manifolding flow distribution in certain circumstances. The CFD simulation results shown in Figure 13 are simply extended to a six-cell serial cooling system and presented in Figure 14. Other heat exchanges among the cells such as conduction through electric connectors are ignored. Cell temperature differences in a module more rapidly increases in the air cooling system proportional to the number of cells connected serially with the coolant channel. Cell-to-cell temperature imbalance mainly comes from the coolant temperature change in coolant channels. Due to the low heat capacity of air, it is difficult to accomplish temperature uniformity inside a cell or between the cells in a module using air for cooling large or high heat generating cells.
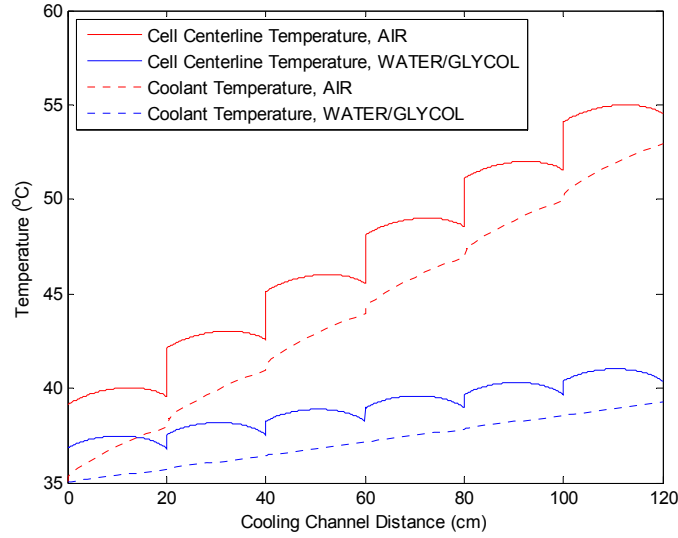
Figure 14: Extended temperature profiles for a six-cell serial cooling system

In order to investigate the time dependent thermal response of battery cooling systems, transient CFD analyses were carried out with a cell specified in Figure 7. An air cooling system and a mineral oil direct liquid cooling system were compared. The systems were operated with the same channel geometry and coolant mass flow rate, $(D_h, \dot{m}_c) = (2.2 \text{ mm}, 1.33 \text{ g/s})$. Initially, each system was in steady state with a heat generation rate of 2 *W*. A system was heated using sudden heat generation (50 *W*) for 2 min. Then, the cell was cooled down to the initial steady state conditions. Coolant inlet temperatures were kept constant at 35 ^{o}C.

Using steady state fully developed relationships shown in Eq.1, channel pressure losses (*ΔP*) are predicted as 109.1 *Pa* and 418.3 *Pa* for the air system and the mineral oil system respectively. On the other hand, heat transfer coefficients are predicted as 59.24 W/m^2K for the air cooled surface and 318.2 W/m^2K for the mineral oil cooled surface. The mineral oil direct contact liquid cooling system is expected to have a much higher heat transfer coefficient than the other coolant systems (direct air and indirect water/glycol) when it is operated at small channel (D_h) and large coolant flow rate ($\dot{m}_c$) at the expense of high pressure loss in the coolant channel. In addition, mineral oil has a higher heat capacity rate ($\dot{m}_c c_p$) than air flow (2.53 *J/Ks* versus 1.34 *J/Ks*), which means it can remove the suddenly released heat from the cell with a smaller increase of coolant temperature. The simulation results showing the transient effect of using high *h* and a high heat capacity coolant system are presented in Figure 15 and Figure 16.
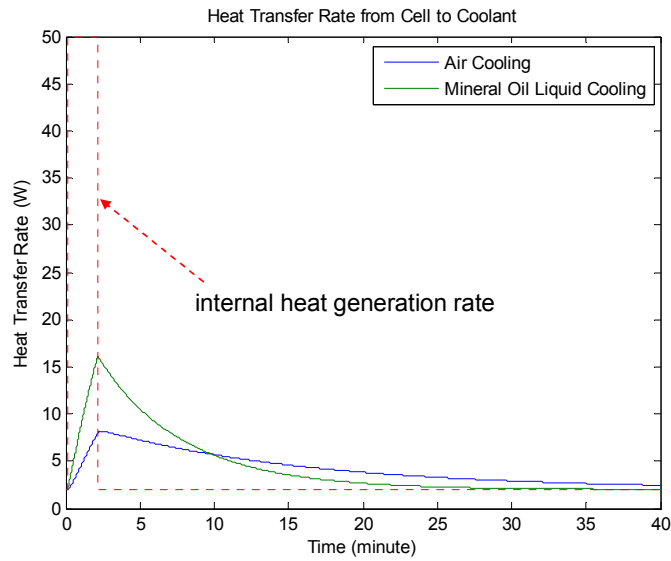
Figure 15: Time variation of heat transfer rates from the cell to the coolant

The heat transfer rates from the cell to the coolant are compared in Figure 15. Due to higher heat transfer coefficient, released heat is more quickly removed from the mineral oil cooled cell. In a high h and high $\dot{m}_c c_p$ system, a large amount of heat can be transferred from cell to coolant with a small temperature increase of the cell while the coolant temperature does not change much.

Time variations of mean temperature of the cell core and mean temperature of the coolant outlet temperature are shown in Figure 16 for both the air and the mineral oil cooling systems. In the mineral oil cooling system, the peak temperature is lower and the cool down time is shorter. The results imply that a high h system is preferred for limiting the maximum peak temperature of a cell and damping out the temperature oscillation in highly transient heat generating battery systems.
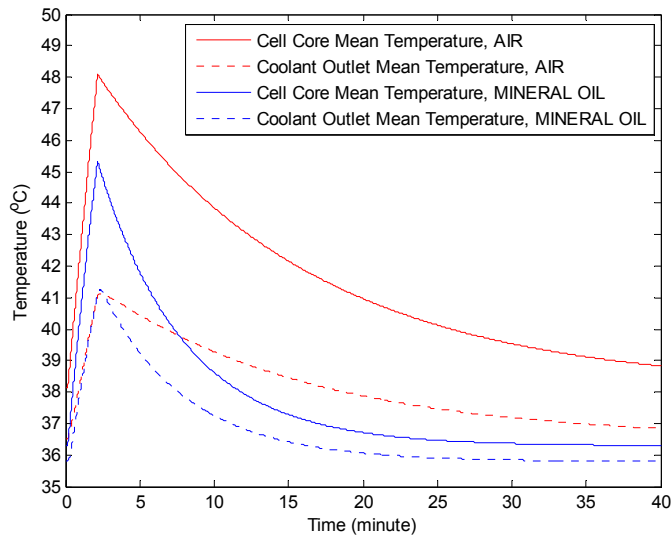

Figure 16: Time variations of mean temperature of the cell core and the coolant outlet temperature

14

Conclusions

In order to achieve performance and cost effective cooling of a battery module/pack for electric or hybrid vehicles, the system thermal responses and their sensitivities are evaluated as a function of controllable system parameters (e.g. D_h and $\dot{m}_c$). For given cell specifications, different types of coolant are examined: air cooling, direct contact liquid cooling using mineral oil, and (indirect) water/glycol jacket cooling system. Trade-off analysis has been performed to identify the optimum operating parameters of cooling systems with given design-limiting conditions.

The simplicity of an air battery cooling system is an advantage over a liquid coolant system. Air cooling could have less mass, has no potential for leaks, needs fewer components, and could cost less. However, the heat transfer coefficient (h) of an air cooling system is lower than that of other coolant systems. Another drawback of an air system comes from its small heat capacity. Due to the small heat capacity of air, it is difficult to accomplish temperature uniformity inside a cell or between the cells in a module using air for cooling large or highly heat generating cells. The temperature difference between coolant air and cell surface (ΔT_2) is sensitive to variations of D_h due to small heat conductivity of air. h is inversely proportional to D_h, while pressure loss in channel (ΔP) is inversely proportional to D_h^3. Therefore, increasing h by reducing D_h is limited by the required blower power. Reducing coolant air temperature change inside a system (ΔT_1) by increasing flow rate ($\dot{m}_c$) is also limited by blower power and size.

Liquid cooling systems are more effective in heat transfer and take up less volume, but the added complexity and cost may outweigh the merits. Maintenance and repair of a liquid cooled pack is more involved and costlier. Indirect liquid cooling, with jackets, is easer to handle than direct liquid cooling. A water/glycol solution for an indirect cooling system has much lower viscosity than dielectric mineral oil for direct liquid cooling. Therefore, increasing the coolant flow rate may not be as severely restricted by the pump power as it is in a mineral oil direct cooling system. Water/glycol has a higher heat capacity. So, the coolant temperature change inside a system can be greatly reduced by using water/glycol as a heat transfer fluid in the system. This means that cell/module temperature uniformity can be effectively achieved even in a serial cooling system if the coolant paths are properly designed. Water/glycol solutions generally have a higher thermal conductivity than oil. However, due to the added thermal resistance between coolant and cell surface, such as jacket wall and air gap, the effective heat transfer coefficient at the cell surface is greatly reduced. Because of the added thermal resistances, h is not as sensitive to the variation of D_h. Since the coolant channel friction head is generally small, D_h is not a critical design parameter in a water/glycol system. A mineral oil direct contact liquid cooling system has a much higher heat transfer coefficient (h) than the other coolant systems when it is operated at small channel (D_h) and large coolant flow rate ($\dot{m}_c$) at the expense of high pressure loss in coolant channel. So, a mineral oil cooling system can be preferred for limiting the maximum peak temperature of a cell and damping out the temperature oscillation in certain circumstances such as in highly transient heat generating battery systems.

CFD analysis captured the axially decreasing heat flux from cell to air which makes the axial gradient of cell surface temperature smaller than that of air temperature. This implies that capturing the internal heat flow paths and thermal resistances inside a cell using a sophisticated three-dimensional cell model is important for the improved prediction of cell/battery thermal behaviors. This paper identified analyses and approaches that engineers should consider when they design battery thermal management systems for vehicles.

Acknowledgments

References

V. Srinivasan and C.Y. Wang, "Analysis of Electrochemical and Thermal Behavior of Li-Ion Cells", *Journal of Electrochemical Soc*iety, Vol. 150, ppA98-A106, 2003.

J. N. Harb , V. H. Johnson and D. Rausen, "Use Of A Fundamentally Based Lead-Acid Battery Model In Hybrid Vehicle Simulations", *Proceedings of Annual Electrochemical Society Conference Seattle*, Washington, Spring 1999.

Ahmad Pesaran, "Battery Thermal Management in EVs and HEVs: Issues and Solutions", *Proceedings of Advanced Automotive Battery Conference*, Las Vegas, Nevada, February 6-8, 2001

Said Al-Hallaj, et. al, "Novel PCM Thermal Management Makes Li-Ion Batteries A viable Option for High Power Applications", *Battery Power Products and Technology Magazine*, November 2004.

Kojiro Ito, et al, "Development of Prismatic Type Nickel / Metal-Hydride Battery for HEVs", *Proceedings of the 20th Electric Vehicle Symposium*, Long Beach, CA, November 2003.

Shuichi Nagata, et. al, "Development of a New Battery System for Hybrid Vehicles" *Proceedings of the 20th Electric Vehicle Symposium*, Long Beach, CA, November 2003.

Authors

Gi-Heon Kim, Post-Doctoral Researcher, National Renewable Energy Laboratory, 1617 Cole Blvd, MS 1633, Golden, CO, 80401, telephone 303-275-4437, fax 303-275-4415, gi_heon_kim@nrel.gov

Dr. Gi-Heon Kim has worked as a post-doctoral researcher with the Advanced Vehicle Systems group at NREL since 2004. His recent research interests in advanced vehicle energy storage system tasks include development of a three dimensional Li-Ion battery thermal abuse model and HEV/EV battery thermal management system modeling. Another recent research topic is alternative fuel based diesel after-treatment systems. His expertise is in heat and mass transfer, fluid mechanics, turbulence, combustion, reacting flows and computational fluid dynamics. Dr. Kim completed a Ph.D. in Mechanical Engineering from Colorado State University with research on performance improvement of natural gas engines. In addition to his Ph.D., Dr. Kim holds an M.S. and B.S. in Mechanical Engineering from Seoul National University in Seoul, Korea.

Ahmad Pesaran, Principal Engineer, National Renewable Energy Laboratory, 1617 Cole Blvd, MS 1633, Golden, CO, 80401, telephone 303-275-4441, fax 303-275-4415, ahmad_pesaran@nrel.gov

Dr. Pesaran joined NREL in 1983 and has been working on various energy systems such as solar cooling, ocean thermal energy conversion, air conditioning, desiccant dehumidification/cooling for buildings and buses, and most recently hybrid electric vehicles. Since 1995, he has been working on hybrid electric vehicle projects. He is currently the project manager for various activities related to battery thermal characterization, battery thermal analysis, and battery modeling and management. Dr. Pesaran holds a B.S. in chemical engineering from Shiraz University, as well as an M.S. in engineering and a Ph.D. in mechanical engineering from UCLA. He is a member of the FreedomCAR Electrochemical Energy Storage Technical Team.

REPORT DOCUMENTATION PAGE

Form Approved
OMB No. 0704-0188

1. REPORT DATE *(DD-MM-YYYY)*	2. REPORT TYPE	3. DATES COVERED *(From - To)*
November 2006	Conference paper	

4. TITLE AND SUBTITLE
Battery Thermal Management System Design Modeling

5a. CONTRACT NUMBER
DE-AC36-99-GO10337

5b. GRANT NUMBER

5c. PROGRAM ELEMENT NUMBER

6. AUTHOR(S)
G.H. Kim and A. Pesaran

5d. PROJECT NUMBER
NREL/CP-540-40446

5e. TASK NUMBER
FC06.6000

5f. WORK UNIT NUMBER

7. PERFORMING ORGANIZATION NAME(S) AND ADDRESS(ES)
National Renewable Energy Laboratory
1617 Cole Blvd.
Golden, CO 80401-3393

8. PERFORMING ORGANIZATION REPORT NUMBER
NREL/CP-540-40446

9. SPONSORING/MONITORING AGENCY NAME(S) AND ADDRESS(ES)

10. SPONSOR/MONITOR'S ACRONYM(S)
NREL

11. SPONSORING/MONITORING AGENCY REPORT NUMBER

12. DISTRIBUTION AVAILABILITY STATEMENT
National Technical Information Service
U.S. Department of Commerce
5285 Port Royal Road
Springfield, VA 22161

13. SUPPLEMENTARY NOTES

14. ABSTRACT *(Maximum 200 Words)*
Looks at the impact of cooling strategies with air and both direct and indirect liquid cooling for battery thermal management.

15. SUBJECT TERMS
battery thermal management; electric vehicles; hybrid electric vehicles

16. SECURITY CLASSIFICATION OF:

a. REPORT	b. ABSTRACT	c. THIS PAGE
Unclassified	Unclassified	Unclassified

17. LIMITATION OF ABSTRACT
UL

18. NUMBER OF PAGES

19a. NAME OF RESPONSIBLE PERSON

19b. TELEPONE NUMBER *(Include area code)*

Standard Form 298 (Rev. 8/98)
Prescribed by ANSI Std. Z39.18